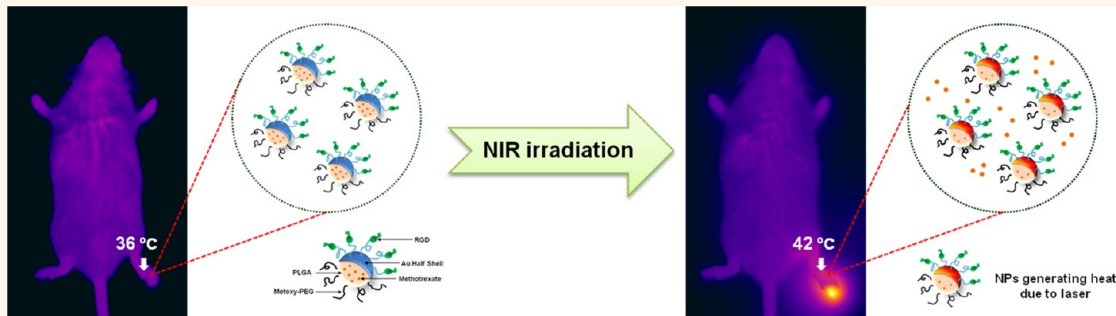


Targeted Chemo-Photothermal Treatments of Rheumatoid Arthritis Using Gold Half-Shell Multifunctional Nanoparticles

Sun-Mi Lee,[†] Hyung Joon Kim,[†] You-Jung Ha,[‡] Young Nyun Park,[§] Soo-Kon Lee,[‡] Yong-Beom Park,^{‡,*} and Kyung-Hwa Yoo^{†,II,*}

[†]Nanomedical Graduate Program, Yonsei University, Seoul 120-749, Korea, [‡]Division of Rheumatology, Department of Internal Medicine, Institute for Immunology and Immunological Disease, Yonsei University College of Medicine, Seoul 120-752, Korea, [§]Department of Pathology, Yonsei University College of Medicine, Seoul 120-752, Korea, and ^{II}Department of Physics, Yonsei University, Seoul 120-749, Korea

ABSTRACT



We have developed RGD-attached gold (Au) half-shell nanoparticles containing methotrexate (MTX) for the treatment of rheumatoid arthritis (RA), where MTX is the most widely used disease-modifying anti-rheumatic drug (DMARD) for the treatment of RA, and RGD peptide is a targeting moiety for inflammation. Upon near-infrared (NIR) irradiation, heat is locally generated due to Au half-shells, and the drug release rate is enhanced, delivering heat and drug to the inflamed joints simultaneously. RA is a chronic inflammatory disease characterized by synovial inflammation in multiple joints within the penetration depth of NIR light. When combined with NIR irradiation, these nanoparticles containing a much smaller dosage of MTX (1/930 of MTX solution) showed greater therapeutic effects than that of a conventional treatment with MTX solution in collagen-induced arthritic mice. This novel drug delivery system is a good way to maximize therapeutic efficacy and minimize dosage-related MTX side effects in the treatment of RA. Furthermore, these multifunctional nanoparticles could be applied to other DMARDs for RA or other inflammatory diseases.

KEYWORDS: rheumatoid arthritis · multifunctional nanoparticles · chemo-photothermal treatment · NIR resonance · photothermally controlled drug delivery

Various near-infrared (NIR) resonant nanomaterials, such as Au nanoshells,^{1,2} Au nanorods,^{3,4} and carbon nanotubes,^{5,6} have been widely studied because they strongly absorb NIR light and produce localized cytotoxic heat upon NIR irradiation. In addition, multifunctional nanoparticles that can deliver both heat and drug simultaneously to the selected region have been also developed.^{7–10} So far, the studies using these nanomaterials have been mainly focused on cancer treatments.^{1–10} However, a limited penetration depth of

NIR light hinders their practical application in the cancer treatments. Here, we explore the use of multifunctional nanoparticles in the treatment of rheumatoid arthritis (RA) that involves small synovial joints within the penetration depth of NIR light. Synovial proliferation of RA resembles solid tumors in many ways, including the leaky nature of the associated blood capillaries;¹¹ thus, multifunctional nanoparticles are expected to be useful for RA treatment.

Rheumatoid arthritis is the most common inflammatory arthritis and is a major cause

* Address correspondence to
kyoo@yonsei.ac.kr,
yongbpark@yuhs.ac.

Received for review March 19, 2012
and accepted November 29, 2012.

Published online November 29, 2012
10.1021/nn301215q

© 2012 American Chemical Society

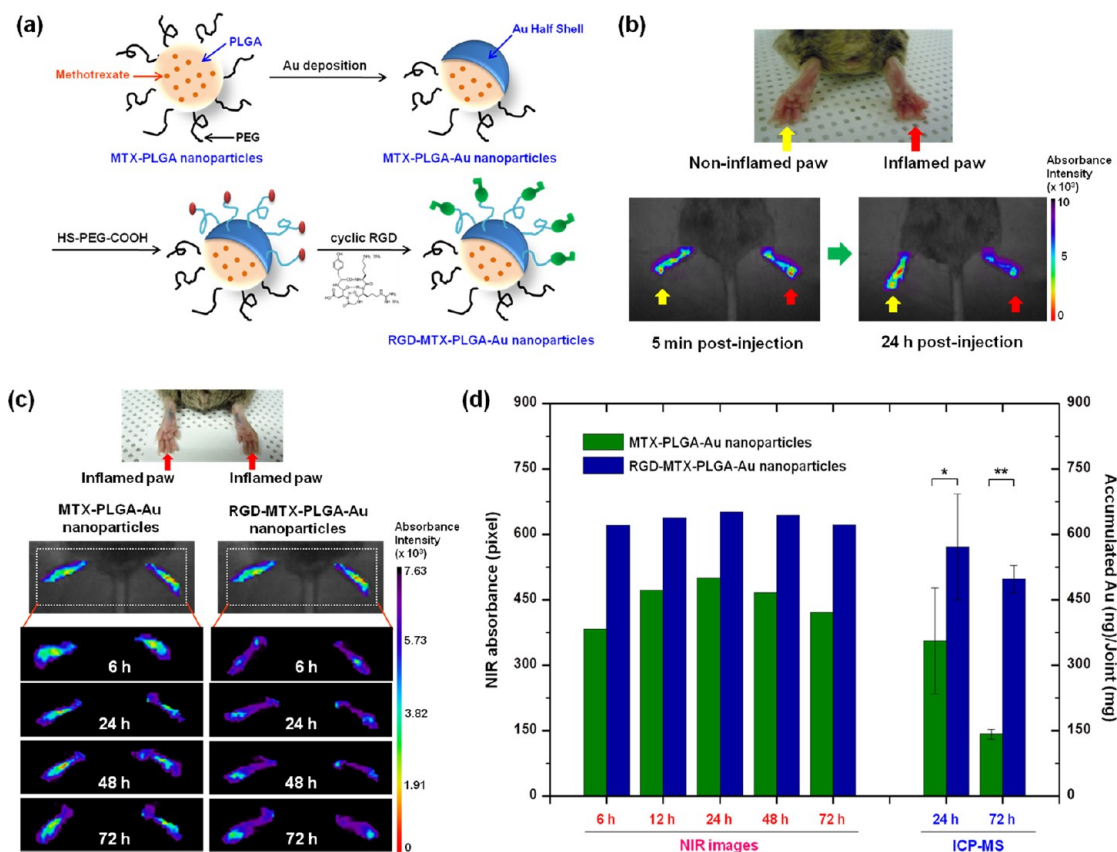


Figure 1. (a) Schematic fabrication process of RGD-MTX-PLGA-Au nanoparticles. (b) *In vivo* NIR absorbance images of inflamed and noninflamed paws in CIA mouse injected intravenously with RGD-MTX-PLGA-Au nanoparticles (150 μ L, 1 mg/mL dispersed in PBS). (c) Time-lapse *In vivo* NIR absorbance images of inflamed paws in CIA mice injected intravenously with MTX-PLGA-Au nanoparticles (150 μ L, 1 mg/mL dispersed in PBS, left column) or RGD-MTX-PLGA-Au nanoparticles (150 μ L, 1 mg/mL dispersed in PBS, right column). (d) Number of pixels in which the absorbance intensity was above 3.82×10^3 au as a function of time for nanoparticle-treated mice (left axis) and the amount of Au accumulated in the inflamed paws extracted from the nanoparticle-treated mice 24 and 72 h after intravenous injection (right axis). The mass of Au was measured using ICP-MS. Data represent mean values for $n = 3$, and the error bars represent standard deviation of the means.

of disability.¹² RA has a progressive disease course with structural damages and worsening functional capacity in the affected joints.¹³ Disease-modifying anti-rheumatic drugs (DMARDs) are the main strategy for the treatment of RA, and methotrexate (MTX) is the most widely used DMARD for the treatment of RA.^{14,15} MTX can be prescribed alone or with other DMARDs or biologic agents for combination therapy. However, despite its good therapeutic efficacy, the long-term administration of MTX may induce serious systemic complications, including infection, hepatitis, and bone marrow suppression.^{16,17} From a clinical point of view, increasing the dose of MTX in RA patients, who have several refractory joints or MTX dose-related side effects, or continuing MTX in patients who have systemic disease, such as interstitial lung disease, viral hepatitis, or bone marrow dysfunction, may provoke more unwanted adverse effects. Therefore, the novel delivery systems to maintain a high concentration of MTX within the joint spaces, which is the main area of inflammation, by administration of small dosage of drugs and to reduce side effects in accordance with

systemic administration of MTX would be an attractive and effective tool for RA treatment.

For the treatment of RA, we developed MTX-loaded poly(DL-lactic-co-glycolic acid) Au half-shell nanoparticles (MTX-PLGA-Au) and conjugated arginine-glycine-aspartic acid (RGD) peptides to the surface of the Au half-shell, where the RGD peptide is a targeting moiety for inflammation.¹⁸ The nanoparticles injected into collagen-induced arthritic (CIA) mice were effectively delivered to the inflamed joints due to RGD peptides conjugated to the nanoparticles, and the accumulation of nanoparticles was enhanced in the inflamed joints. Upon NIR exposure, heat was generated due to Au half-shells and drug was rapidly released from PLGA nanoparticles, allowing photothermally controlled drug delivery. Compared to conventional treatment, the application of multifunctional nanoparticles in CIA mice had superior therapeutic efficacy with a much smaller dosage of MTX.

RESULTS AND DISCUSSION

The multifunctional nanoparticles used in our experiments are shown in Figure 1a. First, we prepared

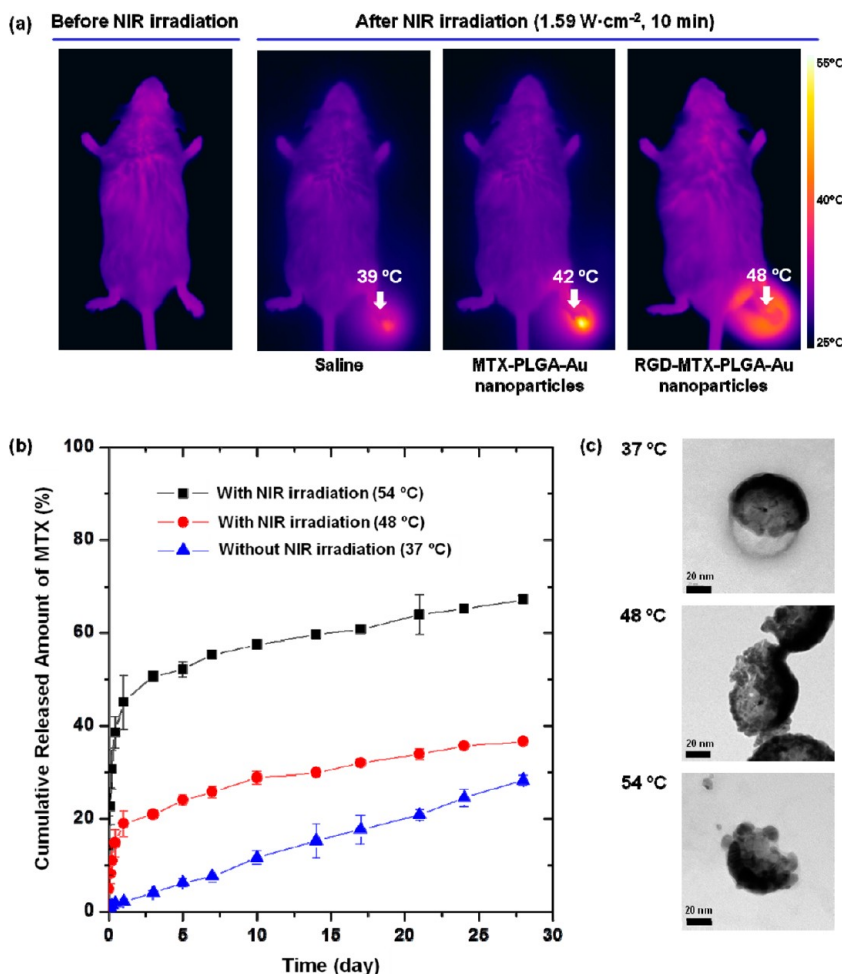


Figure 2. (a) Thermal images of CIA mice treated with saline, MTX-PLGA-Au nanoparticles (150 μ L, 1 mg/mL dispersed in PBS), or RGD-MTX-PLGA-Au nanoparticles (150 μ L, 1 mg/mL dispersed in PBS) before and after NIR exposure (1.59 W/cm², 10 min) of the right paw. (b) Profiles of MTX release from RGD-MTX-PLGA-Au nanoparticles with and without NIR irradiation of 0.38 (48 °C) or 0.53 (54 °C) W/cm² for 10 min at the initial time. Data represent mean values for $n = 3$, and the error bars represent standard deviation of the means. (c) TEM images of RGD-MTX-PLGA-Au nanoparticles measured after MTX release experiments without (top) or with NIR irradiation of 0.38 (48 °C, middle) or 0.53 (54 °C, bottom) W/cm² for 10 min at the initial time.

MTX-loaded PLGA (MTX-PLGA) nanoparticles. Next, Au film (15 nm) was deposited onto the MTX-PLGA nanoparticle monolayer prepared on a Si substrate using a thermal evaporator, resulting in a half-shell structure (MTX-PLGA-Au). After depositing the Au film, Au-deposited MTX-PLGA nanoparticles were released into 1 wt % SH-PEG-COOH solution from the substrate by sonication and collected by centrifugation. For targeted delivery, cyclic RGD peptide, which binds $\alpha_v\beta_3$ integrins expressed on angiogenic vascular endothelial cells at sites of inflammation,^{19,20} was conjugated on the Au surface (RGD-MTX-PLGA-Au). The size of these nanoparticles was 100–115 nm in diameter. The ultraviolet–visible/NIR absorption spectrum of MTX-PLGA-Au or RGD-MTX-PLGA-Au nanoparticles exhibited a pronounced peak at approximately 810 nm due to Au half-shells (Figure S1 in the Supporting Information), suggesting that both nanoparticles can be used for photothermal treatment and *in vivo* NIR absorbance imaging.

In order to evaluate the *in vivo* targeting efficacy of RGD-MTX-PLGA-Au nanoparticles to inflamed joints, we intravenously administered 150 μ L of RGD-MTX-PLGA-Au nanoparticle solution (1 mg/mL) to a CIA mouse. The injected nanoparticles were monitored by measuring *in vivo* NIR absorbance at 5 min and 24 h using the eXplore Optix System (Figure 1b). We noted the color change in the inflamed paw, whereas a significant color change was not observed in the noninflamed paw, indicating that nanoparticles were selectively delivered to and accumulated in the inflamed joint.

CIA mice treated with MTX-PLGA-Au or RGD-MTX-PLGA-Au nanoparticles exhibited a change in *in vivo* absorbance intensity over time due to localization of nanoparticles in the inflamed paws (Figure 1c). The number of pixels with absorbance intensity $\geq 3.82 \times 10^3$ au increased up to 24 h after intravenous administration and then decreased, possibly due to a slow release of nanoparticles by leaky angiogenic vessels (Figure 1d).¹¹ To quantify the accumulation of

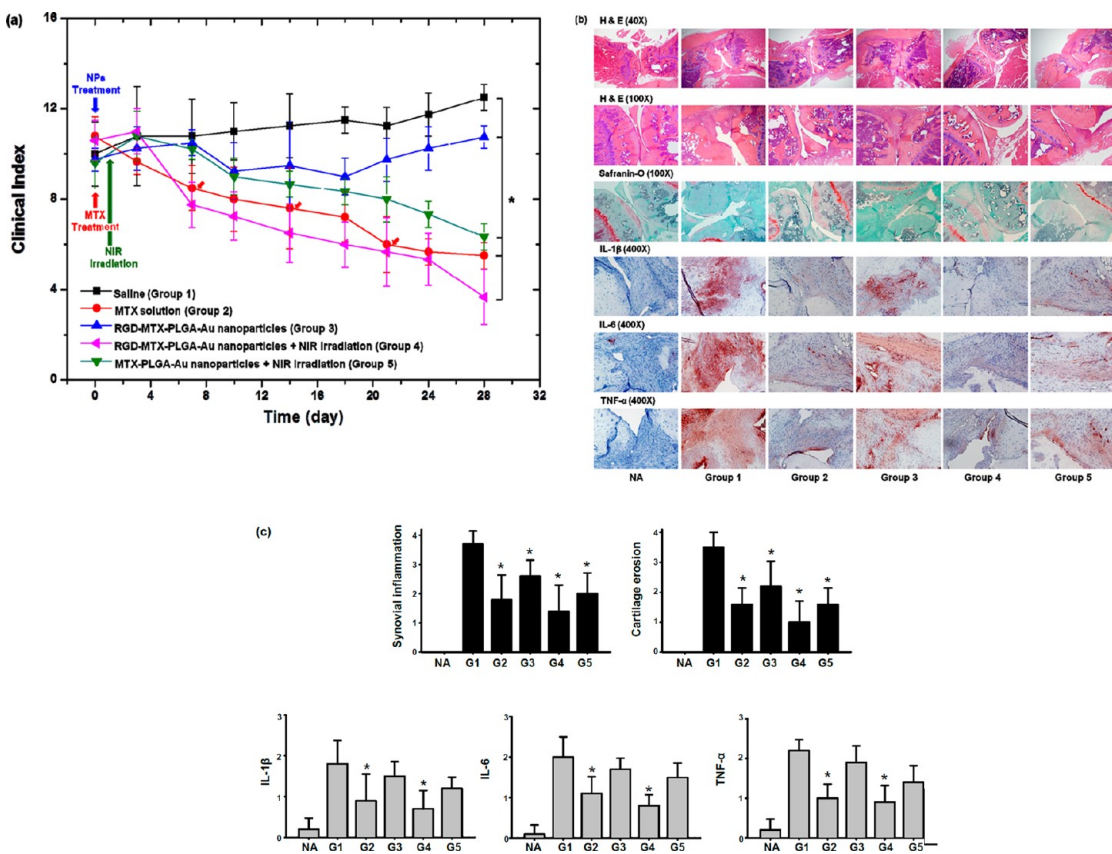


Figure 3. (a) Clinical index versus time for CIA mice injected intravenously with saline (group 1), MTX solution (35 mg/kg \times 4 times, group 2), RGD-MTX-PLGA-Au nanoparticles (0.15 mg/kg of MTX, group 3), RGD-MTX-PLGA-Au nanoparticles (0.15 mg/kg of MTX) with NIR irradiation (1.59 W/cm 2 , 10 min, group 4), or MTX-PLGA-Au nanoparticles (0.15 mg/kg of MTX) with NIR irradiation (1.59 W/cm 2 , 10 min, group 5). The clinical index is the sum of the clinical scores for four paws (maximum scores = 16). The evaluated paws were scored from 0 to 4 according to the following scale: 0 = no evidence of erythema and swelling, 1 = erythema and mild swelling, 2 = erythema and mild swelling extending from the ankle to the tarsals, 3 = erythema and moderate swelling extending from the ankle to metatarsal joints, and 4 = erythema and severe swelling encompassing the ankle, foot, and digits or ankylosis of the limb. Error bars represent standard deviation ($n = 5$). Clinical indices were significantly different among groups ($^*p < 0.0001$). Multivariate linear mixed models were used to calculate summary estimates at different time points. (b) Histology of joint tissues extracted from a normal mouse (NA) and CIA mice 28 days after each treatment. H&E (synovial inflammation, original magnification, $\times 40$, $\times 100$), safranin-O (cartilage erosion, original magnification, $\times 100$), and immunohistochemical staining for IL-1 β , IL-6, and TNF- α (original magnification, $\times 400$) stained representative joint sections from experiment. (c) Semiquantitative analysis of histopathological evaluation (synovial inflammation and cartilage erosion) and immunohistochemical staining for IL-1 β , IL-6, and TNF- α in CIA mice. The bars represent the standard deviation. Asterisks (*) represent significance compared to untreated mice with $^*p < 0.05$ ($n = 5$).

nanoparticles in the inflamed joints, we measured the mass of Au in the inflamed paws 24 and 72 h post-injection using an inductively coupled plasma mass spectrometer (ICP-MS) (Figure 1d). In two paws of the CIA mice treated with RGD-MTX-PLGA-Au nanoparticles, 0.23 μ g of Au was found at 24 h, corresponding to 0.9% of the injected nanoparticles, whereas 0.16 μ g of Au (0.7%) was measured in the inflamed paws treated with MTX-PLGA-Au nanoparticles. These results indicate that nanoparticles were more effectively delivered to the inflamed region *via* active targeting compared to passive targeting.

Heat is locally generated by NIR irradiation because the Au half-shells have an absorption peak in the NIR region. To determine the temperature increase upon NIR exposure, we measured the temperature of CIA mice treated with saline, MTX-PLGA-Au nanoparticles or RGD-MTX-PLGA-Au nanoparticles 24 h post-injection using a

thermal imaging camera (FLIR-T250, FLIR, Sweden) when the right inflamed paw was exposed to 1.59 W/cm 2 NIR light for 10 min using a laser diode ($\lambda \approx 808$ nm) (Figure S2a). Before NIR exposure, the temperature was approximately 36 °C over the whole body, corresponding to the body temperature of the mouse. However, after 10 min of NIR irradiation, the temperature of the irradiated paw increased to 39, 42, and 48 °C for the mice treated with saline, MTX-PLGA-Au nanoparticles, and RGD-MTX-PLGA-Au nanoparticles, respectively (Figure 2a). These temperatures are not high enough to induce irreversible tissue damage. The regions that were not exposed to NIR light experienced a smaller increase in temperature (Figure S2b), confirming that heat can be delivered to only the inflamed region using a laser-guided light source.

Biodegradable PLGA nanoparticles degrade more rapidly with increasing temperature.^{8,21} In order to study

the effect of 10 min NIR irradiation on the MTX release rate, we measured the release profile at 37 °C with and without 10 min NIR irradiation (Figure 2b). The release rate of MTX from nanoparticles was nearly constant without NIR irradiation, resulting in a linear release profile. However, 10 min NIR irradiation induced a burst release of MTX for 12 h, after which the release rate was reduced. These results indicate that the MTX release rate from nanoparticles can be controlled by NIR light.

After measuring MTX release, the nanoparticle morphology was examined using a transmission electron microscope (TEM) (Figure 2c). In the absence of NIR light, PLGA nanoparticles were not degraded completely and the PLGA that was not covered with Au was partly seen. In contrast, when nanoparticles were irradiated with NIR light, PLGA nanoparticles were mostly degraded and only Au half-shell nanoparticles were clearly observed, supporting photothermally controlled drug release.

In order to investigate the therapeutic effects of multifunctional nanoparticles, we carried out comparative efficacy studies (Figure 3a and Figure S3 and movies S1 and S2 in Supporting Information). CIA mice were divided into five groups ($n = 5$ mice per group), and 150 μ L of each treatment was administered via intravenous tail injection, as summarized in Table 1. For MTX, 35 mg/kg was injected four times every week. In the mice treated with RGD-MTX-PLGA-Au nanoparticles (0.15 mg/kg MTX) without NIR irradiation (group 3), the clinical indices slowly decreased until about day 20 and then increased again, though they were lower than those of the saline-treated mice (group 1). However, when the mice were treated with RGD-MTX-PLGA-Au nanoparticles (0.15 mg/kg MTX) and exposed to 1.59 W/cm² NIR light for 10 min at 24 h after intravenous injection (group 4), the clinical indices were lower than those of the mice treated with free MTX solution four times every week (group 2), which might be due to photothermally controlled drug release. For group 3, MTX was slowly released from nanoparticles (Figure 2b); therefore, the released dosage of MTX was probably at a subtherapeutic level, resulting in the small therapeutic effects. In contrast, the temperature of the inflamed paw exposed to NIR light increased to 48 °C (Figure 2a), leading to a release of more than 20% of the loaded MTX within 12 h (Figure 2b). This dosage of MTX released locally in the inflamed paw was likely above the therapeutic dose, so high therapeutic efficacies were obtained for group 4. We noted that the nanoparticles injected into group 4 contained only 0.15 mg/kg of MTX, which is 1/930 of the dose in group 2, suggesting that the nanoparticle-based treatment would contribute to minimizing dosage-related side effects. We also investigated the effect of NIR power density on therapeutic efficacy (Figure S4). The lowest clinical indices were obtained with 1.59 W/cm² NIR irradiation for 10 min.

TABLE 1. Summary of Treatments Applied to CIA Mice for Comparative Study of Therapeutic Efficacy

group	administered content ^a	dosage of MTX (mg/kg)	NIR light (W/cm ²) ^b
1	saline		
2	MTX solution	35 × 4 times	
3	RGD-MTX-PLGA-Au nanoparticles	0.15	
4	RGD-MTX-PLGA-Au nanoparticles	0.15	1.59
5	MTX-PLGA-Au nanoparticles	0.15	1.59

^aAdministered content was injected intravenously by tail vein in a volume 150 μ L with a nanoparticle concentration of 1 mg/mL. ^bThe arthritis was exposed to NIR light for 10 min with a laser diode ($\lambda = 808$ nm) at 24 h post-injection.

When the inflamed paws were exposed to 1.91 W/cm² NIR light, the clinical index was not reduced. These findings implied that moderate heat might relieve RA, but too much heat aggravated it.

For comparison, the mice were also treated with MTX-PLGA-Au nanoparticles (0.15 mg/kg), followed by 10 min NIR irradiation (1.59 W/cm², group 5). Although the same dosage of MTX and the same NIR light power were applied as in group 4, higher clinical indices were found in group 5 than in group 4 (Figure 3a). To obtain therapeutic effects comparable to group 2, a higher dosage of MTX-PLGA-Au nanoparticles (0.2 mg/kg) and higher NIR power (1.96 W/cm²) were required (Figure S5). These results demonstrate that higher therapeutic efficacy can be achieved by chemo-photothermal treatment combined with targeted delivery compared to the treatment without targeted delivery.

To confirm the therapeutic effects of the targeted chemo-photothermal treatment, we performed histological examinations of joints 28 days after intravenous injection (Figure 3b). Group 1 exhibited marked synovial inflammation and cartilage erosion, whereas the extent of synovial inflammation and cartilage erosion was reduced in groups 2 and 4 (Figure 3c). Pro-inflammatory cytokines, including IL-1 β , IL-6, and TNF- α , are centrally involved in the pathogenesis of RA, and their expressions are closely related to the inflammatory activity of RA. Immunohistochemical staining showed increased TNF- α , IL-6, and IL-1 β expression around the joint in group 1, whereas they were significantly decreased in groups 2 and 4 (Figure 3c). There were no significant differences between group 2 and group 4. We performed three-dimensional micro-CT to assess bony changes in the paws of CIA mice (Figure S6, Supporting Information). The paws of saline-treated CIA mice exhibited severe bone destruction. On the other hand, the bony structures were relatively well preserved in the paws of groups 2 and 4. To determine the extent of bone preservation, the bone volume of the paws of CIA mice was measured. The bone volume in the treated group tended to be better preserved.

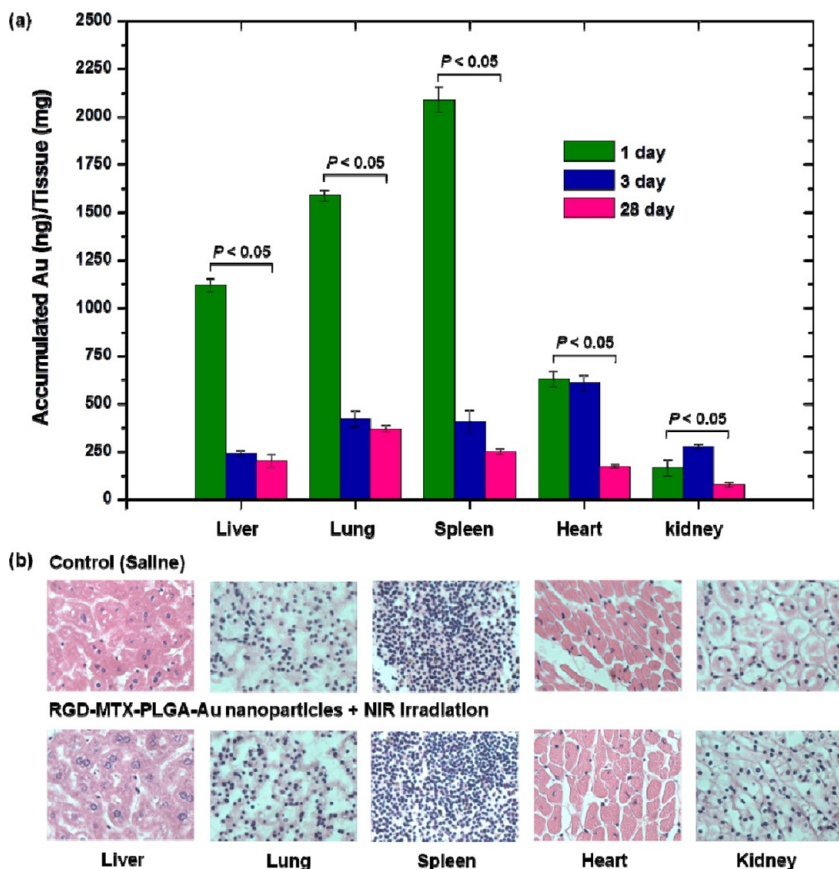


Figure 4. (a) Tissue distribution of nanoparticles in major organs at different times. The amount of Au was measured by ICP-MS (*t*-test, one-tailed, paired, liver, $p = 0.026$; lung, $p = 0.005$; spleen, $p = 0.031$; heart, $p = 0.002$; kidney, $p = 0.039$). Error bars represent standard deviation ($n = 5$). (b) Histological sections of major organs extracted 28 days after intravenous injection of saline (top) or RGD-MTX-PLGA-Au nanoparticles with NIR irradiation (bottom, group 4). Images were acquired at $400\times$ magnification.

An important concern for nanoparticle-based treatments is whether the injected nanoparticles accumulate in organs or are cleared from the body. To investigate the biodistribution of RGD-MTX-PLGA-Au nanoparticles, we measured the Au accumulated in major organs 1, 3, and 28 days after intravenous injection using ICP-MS (Figure 4a). Nanoparticles were efficiently taken up by the liver, lung, and spleen that are related with the reticuloendothelial system (RES), with less accumulation in the kidney or heart. However, most nanoparticles were cleared from the body after 28 days. In order to study the normal tissue toxicity caused by the nanoparticles, we carried out histological examinations of major organs 28 day postinjection (Figure 4b). No tissue damage was evident compared to the nanoparticle-free control, implying that nanoparticles accumulating in major organs did not induce *in vivo* toxicity.

CONCLUSION

We studied the therapeutic effects of RGD-MTX-PLGA-Au nanoparticles in CIA mice. When the nanoparticles were injected intravenously into the CIA mice, *in vivo* NIR absorbance images revealed that the nanoparticles selectively accumulated in the inflamed region. Upon NIR irradiation (1.59 W/cm^2 , 10 min), the temperature of the inflamed paw increased to $48\text{ }^\circ\text{C}$, leading to the burst release of MTX from the nanoparticles. Compared to conventional treatment with MTX, the RGD-MTX-PLGA-Au nanoparticle-based treatment combined with NIR irradiation had greater therapeutic efficacy with a much smaller dosage of MTX in the nanoparticles. These results demonstrate that the targeted chemo-photothermal treatment using multifunctional nanoparticles is a useful and effective strategy for maximizing the therapeutic efficacy and minimizing dosage-related side effects in the treatment of RA.

METHODS

Materials. Poly(DL-lactic-co-glycolic acid) (PLGA; L/G molar ratio = 50:50; $M_w = 20\,000$) was purchased from Wako (Japan).

Monothiol poly(ethylene glycol) with a carboxylic acid group (SH-PEG-COOH, $M_w = 5000$) was purchased from Creative PEG-Works (USA). The cyclic RGD (cyclic Arg-Gly-Asp- D -Tyr-Lys)

peptide was purchased from FutureChem Co. Ltd. (Seoul, Korea). Methotrex, Pluronic F-127, and carbodiimide hydrochloride (EDC) were purchased from the Sigma-Aldrich Chemical Co. (St. Louis, MO, USA).

Fabrication of RGD-MTX-PLGA-Au Nanoparticles. We prepared MTX-PLGA nanoparticles as previously reported method^{9,10} and then deposited 15 nm thick Au film onto an MTX-PLGA nanoparticle monolayer prepared on a Si substrate using a thermal evaporator. After depositing the Au film, Au-deposited MTX-PLGA nanoparticles were released into 1 wt % SH-PEG-COOH solution from the substrate by sonication and collected by centrifugation. The collected carboxylic-acid-terminated MTX-PLGA-Au nanoparticles (74.6 μ M) and EDC (746.7 μ M) were dissolved in 25 mL of 0.2 M phosphate buffer (pH 6.0) and stirred at room temperature. After 30 min, cyclic RGD (74.6 μ M) in 3 mL of distilled water was added and the pH value of the reaction mixture adjusted to 8.0 by adding 0.5 M NaOH. The reaction mixture was then left at room temperature for the RGD peptides to bind covalently to the COOH group of the SH-PEG-COOH chains immobilized on the surface of the Au half-shells. After 12 h, RGD-MTX-PLGA-Au nanoparticles were collected by centrifugation for 30 min at 100 000 rpm; the supernatant containing unreacted cyclic RGD was discarded. The resulting RGD-MTX-PLGA-Au nanoparticles were characterized using a ¹H NMR spectrometer (300 MHz, DMSO-*d*₆, 25 °C, TMS, Varian Gemini-300 spectrometer) with δ values of 8.1–8.6 (–NH(NH₂)=NH of cyclic RGD), 5.2 (m, CH of PLGA), 3.6 (s, CH₂ of PEG), and 1.5 (d, CH₃ of PLGA).

Characterization of RGD-MTX-PLGA-Au Nanoparticles. The size and zeta-potential of prepared nanoparticles dispersed in an aqueous medium were measured at 25 °C by dynamic light scattering (DLS, Zetasizer Nano ZS, Malvern Instruments Ltd.) as summarized in Table S1. To determine the encapsulation efficiency, which was expressed as the percentage of the actual amount of MTX loaded in nanoparticles relative to the theoretical amount of MTX, was estimated to be about 2.5%.

To determine the RGD content in RGD-MTX-PLGA-Au nanoparticles, the conjugate sample was dissolved in distilled water and dried for hydrolysis. The sample was hydrolyzed in 6 N HCl at 110 °C for 24 h and then derived with phenylisothiocyanate (PITC). After microcentrifugation of the derived conjugate sample, its supernatant was filtered through a 0.45 μ m filter and analyzed by high-pressure liquid chromatography (HPLC) using a C₁₈ column (Waters Nova-Pak C₁₈, 3.9 × 300 mm, 4 μ m) equipped with an oven (46 °C), HP 1100 series injector (Autosampler), binary pump, and variable wavelength detector. The solvent system (solvent A, 1.4 mM NaHAc, 0.1% TEA, 6% CH₃CN, pH 6.1; solvent B, 60% CH₃CN) consisted of a linear gradient (0–100%) of solvent B. To determine the amount of each amino acid, the samples were detected at 254 nm at a flow rate of 1.0 mL/min with injection volumes of 4 μ L for the standard curve and 10 μ L for samples. The density of the immobilized peptides in RGD-MTX-PLGA-Au nanoparticles was 41.8 μ g peptide/mg nanoparticles.

In Vitro Drug Release. For *in vitro* MTX release experiments, 10 mg of RGD-MTX-PLGA-Au nanoparticles was loaded into a 1000 Da cutoff membrane dialysis tube (Tube-O-DIALYZER, G-Biosciences, St. Louis, MO, USA). The tubes were immersed in a transparent vial filled with 10 mL of PBS (pH 7.4, 10 mM) under mild constant shaking (150 rpm). The release experiments were performed with and without NIR irradiation of 0.38 or 0.53 W/cm for 10 min at the initial time of the experiment at 37 °C. The release medium was replaced with fresh PBS at determined intervals to maintain release conditions. The amount of released MTX was measured by UV–vis spectrophotometry at 304 nm. All measurements were performed in triplicate.

Induction and Treatment of Rheumatoid Arthritis. All animals were treated in accordance with the guidelines and regulations for the use and care of animals at Yonsei University, Seoul, Korea. First, an intradermal injection of 200 μ g of bovine type II

collagen (Condrex, Redmond, USA) emulsified in 200 μ g of complete Freund's adjuvant (Condrex, Redmond, USA) was given in the base of the tail of male DBA/1J mice (8 weeks old, SLC Inc., Shizuoka, Japan) to induce rheumatoid arthritis. Next, a booster intradermal injection of 100 μ g of bovine type II collagen in incomplete Freund's (Condrex, Japan) was given to mice at 21 days after the primary immunization. When arthritis was fully developed, saline (group 1), MTX solution (group 2), RGD-MTX-PLGA-Au nanoparticles (groups 3 and 4), or MTX-PLGA-Au nanoparticles (group 5) were intravenously administered to the mice, and groups 4 and 5 were exposed to 1.59 W/cm² NIR light for 10 min at 1 day after intravenous injection of nanoparticles (*n* = 5 mice each group). After injection, the mice were observed twice per week for 4 weeks. The clinical index is the sum of the clinical scores for four paws (maximum scores = 16). The evaluated paws were scored from 0 to 4 according to the following scale: 0 = no evidence of erythema and swelling, 1 = erythema and mild swelling, 2 = erythema and mild swelling extending from the ankle to the tarsals, 3 = erythema and moderate swelling extending from the ankle to metatarsal joints, and 4 = erythema and severe swelling encompassing the ankle, foot, and digits or ankylosis of the limb.

In Vivo NIR Imaging. MTX-PLGA-Au nanoparticles or RGD-MTX-PLGA-Au nanoparticles (150 μ L, 1 mg/mL dispersed in PBS) were injected intravenously into the CIA mice. The mice were anesthetized with Zoletil50/Rompum (v/v = 3), a short acting anesthetic, and maintained during the imaging process. NIR absorbance images were obtained with an eXplore Optix System (Advanced Research Technologies Inc., Montreal, Canada). The absorbance at 710–750 nm was detected through a fast photomultiplier tube (Hamamatsu, Japan) and a time-correlated single-photon counting system (Becker and Hickl GmbH, Berlin, Germany). All data were calculated using the region-of-interest (ROI) function of the analytical workstation software.

Histology Study. The mice were anesthetized and sacrificed 28 days after each treatment. Joints were removed for histopathological examination and fixed in 10% buffered formalin saline at 4 °C for 1 week. The joints were decalcified in Calci-Clear Rapid solution (National Diagnostics, Atlanta, USA), and specimens were processed for paraffin embedding. Joint tissues were embedded in paraffin blocks, and 5 μ m thick paraffin sections were mounted on a glass slide for hematoxylin and eosin (H&E) and safranin-O staining. The joint sections were scored for changes in synovial inflammation and cartilage erosion, all on a scale of 0–4, which were evaluated as previously described.²² Deparaffinized sections were incubated with specific antibodies directed against IL-1 β , IL-6 (Santa Cruz Biotechnology, Santa Cruz, CA, USA), or TNF- α (Hycult Biotechnology, Uden, The Netherlands), followed by the appropriate peroxidase/DAB secondary antibodies (DAKO, Glostrup, Denmark). Expression of the different cytokines in the synovial tissue was scored semiquantitatively on a 4-point scale.²³ A score of 0 represented no expression, 1 mild expression, 2 moderate expression, and 3 abundant expression of a cytokine. All histologic analyses were performed independently and blindly by two individual assessors, and the average of their scores was calculated.

For histological assessment of normal organ tissues, portions of the heart, kidney, liver, spleen, and lung were extracted 28 days after the injection of saline or RGD-MTX-PLGA-Au nanoparticles with NIR exposure (group 4). Tissue sections were prepared as described above and stained with hematoxylin and eosin.

Microcomputed Tomography (CT). Each experimental mice paws were scanned using micro-CT system (NFR Polarys-G90, Nano-focusray Int, Iksan, Korea). Images were acquired at 80 kVp, 150 mA, and 5 s/frame, with 360 views. The estimated radiation dose was approximately 6.9 mGy using image acquisition protocol. Scanned paws reconstructed into the three-dimensional structure and evaluated by NFR Polarys software (Exxim Computing Corporation, Pleasanton, USA). To confirm volumetric change of arthritis joints, three-dimensional bone volume (BV) including phalanges and metatarsal bones was measured using Aquarius software (version 4.4.6, TeraRecon, Inc.).

Biodistribution and Clearance. RGD-MTX-PLGA-Au nanoparticles (150 μ L, 1 mg/mL dispersed in PBS) were administered intravenously into CIA mice ($n = 3$). The mice were sacrificed 1, 3, or 28 days after injection and the major organs (liver, heart, spleen, kidney, joint, and lung) removed from each mouse. Tissue samples were placed in a mixed acid matrix of aqua regia and heated overnight at 80–90 °C. After additional heating at 130–140 °C for 2 h, the organic compounds were completely removed and only ionized Au remained. This residue was dissolved in 1 mL of 0.5 M HCl and analyzed by ICP-MS (Agilent 7500C).

Statistical Analysis. All results were expressed as the mean \pm standard deviation. When there was sufficient information for every time point, multivariate linear mixed models were used to calculate summary estimates at different time points. Statistical significance was considered $p < 0.05$. All analyses were performed using SAS (version 9.2.4, SAS Institute Inc., Cary, NC, USA).

Conflict of Interest: The authors declare no competing financial interest.

Acknowledgment. This study has been financially supported by MHW through the Korean Health Technology R&D Project (Grant No. A110905) and by MEST through the National Research Foundation of Korea (Grant Nos. 2011-0017486 and 2011-005966).

Supporting Information Available: Additional figures and videos as described in the text. This material is available free of charge via the Internet at <http://pubs.acs.org>.

REFERENCES AND NOTES

1. Loo, C.; Lowery, L.; Halas, N.; West, J.; Drezek, R. Immuno-targeted Nanoshells for Integrated Cancer Imaging and Therapy. *Nano Lett.* **2005**, *5*, 709–711.
2. Hirsch, L. R.; Stafford, R. J.; Bankson, J. A.; Sersher, S. R.; Rivera, B. R.; Price, E.; Hazle, J. D.; Halas, N. J.; West, J. L. Nanoshell-Mediated Near-Infrared Thermal Therapy of Tumors under Magnetic Resonance Guidance. *Proc. Natl. Acad. Sci. U.S.A.* **2003**, *100*, 13549–13554.
3. Huang, X.; El-Sayed, I. H.; Qian, W.; El-Sayed, M. A. Cancer Cell Imaging and Photothermal Therapy in the Near-Infrared Region by Using Gold Nanorods. *J. Am. Chem. Soc.* **2006**, *128*, 2115–2120.
4. Hauck, T. S.; Jennings, T. L.; Yatsenki, T.; Kumaradas, J. C.; Chan, W. C. W. Enhancing the Toxicity of Cancer Chemotherapeutics with Gold Nanorod Hyperthermia. *Adv. Mater.* **2008**, *20*, 3832–3838.
5. Kam, N. W. S.; O'Connell, M.; Wisdom, J. A.; Dai, H. Carbon Nanotubes as Multifunctional Biological Transporters and Near-Infrared Agents for Selective Cancer Cell Destruction. *Proc. Natl. Acad. Sci. U.S.A.* **2005**, *102*, 11600–11605.
6. Moon, H. K.; Lee, S. H.; Choi, H. C. *In Vivo* Near-Infrared Mediated Tumor Destruction by Photothermal Effect of Carbon Nanotubes. *ACS Nano* **2009**, *3*, 707–713.
7. Park, H.; Yang, J.; Seo, S.; Kim, K.; Suh, J.; Kim, D.; Haam, S.; Yoo, K.-H. Multifunctional Nanoparticles for Photothermal Controlled Drug Delivery and Magnetic Resonance Imaging Enhancement. *Small* **2008**, *4*, 192–196.
8. Park, H.; Yang, J.; Lee, J.; Haam, S.; Choi, I. H.; Yoo, K.-H. Multifunctional Nanoparticles for Combined Doxorubicin and Photothermal Treatments. *ACS Nano* **2009**, *3*, 2919–2926.
9. Lee, S. M.; Park, H.; Yoo, K.-H. Synergistic Cancer Therapeutic Effects of Locally Delivered Drug and Heat Using Multifunctional Nanoparticles. *Adv. Mater.* **2010**, *22*, 4049–4053.
10. Lee, S. M.; Park, H.; Choi, J. W.; Park, Y. N.; Yun, C. O.; Yoo, K.-H. Multifunctional Nanoparticles for Targeted Chemo-photothermal Treatment of Cancer Cells. *Angew. Chem., Int. Ed.* **2011**, *50*, 7581–4586.
11. Levick, J. R. Permeability of Rheumatoid and Normal Human Synovium to Specific Plasma Proteins. *Arthritis Rheum.* **1981**, *24*, 1550–1560.
12. Firestein, G. S. Evolving Concepts of Rheumatoid Arthritis. *Nature* **2003**, *423*, 356–361.
13. Pincus, T.; Callahan, L. F.; Sale, W. G.; Brooks, A. L.; Payne, L. E.; Vaughn, W. K. Severe Functional Declines, Work Disability, and Increased Mortality in Seventy-Five Rheumatoid Arthritis Patients Studied over Nine Years. *Arthritis Rheum.* **1984**, *27*, 864–872.
14. Saag, K. G.; Teng, G. G.; Patkar, N. M.; Anuntiyo, J.; Finney, C.; Curtis, J. R.; Paulus, H. E.; Mudano, A.; Pisu, M.; Elkins-Melton, M.; et al. American College of Rheumatology Recommendations for the Use of Nonbiologic and Biologic Disease-Modifying Anti-rheumatic Drugs in Rheumatoid Arthritis. *Arthritis Rheum.* **2008**, *59*, 762–784.
15. Smolen, J. S.; Landewé, R.; Breedveld, F. C.; Dougados, M.; Emery, P.; Cecile Gaujoux-Viala, C.; Gorter, S.; Knevel, R.; Nam, J.; Schoels, M.; et al. EULAR Recommendations for the Management of Rheumatoid Arthritis with Synthetic and Biological Disease-Modifying Antirheumatic Drugs. *Ann. Rheum. Dis.* **2010**, *69*, 964–975.
16. Schnabel, A.; Gross, W. L. Low-Dose Methotrexate in Rheumatic Diseases—Efficacy, Side Effects, and Risk Factors for Side Effects. *Semin. Arthritis Rheum.* **1994**, *23*, 310–327.
17. van Ede, A. E.; Laan, R. F. J. M.; Blom, H. J.; De Abreu, R. A.; van de Putte, L. B. A. Methotrexate in Rheumatoid Arthritis: An Update with Focus on Mechanisms Involved in Toxicity. *Semin. Arthritis Rheum.* **1998**, *27*, 277–292.
18. Hynes, R. O. A Reevaluation of Integrins as Regulators of Angiogenesis. *Nat. Med.* **2002**, *8*, 918–921.
19. Johnson, E. A.; Haines, G. K.; Harlow, L. A.; Koch, A. E. Adhesion Molecule Expression in Human Synovial Tissue. *Arthritis Rheum.* **1993**, *36*, 137–146.
20. Walsh, D. A.; Wade, M.; Mapp, P. I.; Blake, D. R. Focally Regulated Endothelial Proliferation and Cell Death in Human Synovium. *Am. J. Pathol.* **1998**, *152*, 691–702.
21. Zolnik, B. S.; Leary, P. E.; Burgess, D. J. Elevated Temperature Accelerated Release Testing of PLGA Microspheres. *J. Controlled Release* **2006**, *112*, 293–300.
22. Camps, M.; Rückle, T.; Ji, H.; Ardisson, V.; Rintelen, F.; Shaw, J.; Ferrandi, C.; Chabert, C.; Gillieron, C.; Françon, B.; et al. Blockade of PI₃K_γ Suppresses Joint Inflammation and Damage in Mouse Models of Rheumatoid Arthritis. *Nat. Med.* **2005**, *11*, 936–943.
23. Lee, S. W.; Kim, J. H.; Park, Y. B.; Lee, S. K. Bortezomib Attenuates Murine Collage-Induced Arthritis. *Ann. Rheum. Dis.* **2009**, *68*, 1761–1767.